# Research on the Influence of Distance Between the Improved Ag/AgCl RE and the steel on the Corrosion Evaluation in Concrete

*Ming Jin[1], Linhua Jiang[1,2,*], Shuya Bai[1], Shaobo Jiang[1], Chuansheng Xiong[1], Zijian Song[1]*

[1] College of Mechanics and Materials, Hohai University, Nanjing 210098, PR China
[2] National Engineering Research Center of Water Resource Efficient Utilization and Engineering Safety, 1 Xikang Rd., Nanjing 210098, PR China
[*]E-mail: lhjiang@hhu.edu.cn

In this paper, the impact of the distance between the improved Ag/AgCl RE and the steel in concrete on the corrosion monitoring exposed to the accelerated drying/wetting cycles has been investigated. The 3D morphology of steel surface was obtained by 3D video microscope. Results showed that the corrosion rate of steel determined by MS 1 was more accurate and reliable than those by MS 2 and 3. The $C_{red}$ value measured by MS 1 was clearly lower than that determined by MS 2 and MS 3. However, the $C_f$ value measured through MS 1was in higher side compared to that by MS 2 and MS 3. Therefore, it was recommended to place the corrosion monitoring system close to the working electrode as soon as possible in order to obtain the precise measurements of corrosion condition of steel. Beside, the half-cell potential (HCP) of steel in concrete with respect to MS 1 are -185, -185 to -297, -297 to -455 and -455 mV for passive, low to moderate corrosion rate, moderate to high corrosion rate and high corrosion rate conditions.

## 1. INTRODUCTION

Reinforced concrete is concrete in which reinforced steels have been integrated to improve the properties of concrete. The generation of a thin passive film on the steel surface will occur due to the strong alkaline environment in concrete. Nevertheless, breakdown of the protective film happens because of the process of carbonation and the ingressive of chloride ion[1-3]. Thus, the mechanical performances and service life of concrete are affected due to the development of steel corrosion. Based on this, the monitoring and evaluation of the conditions of steel in concrete have significant senses.

Song and Saraswathy[4] introduced several techniques applied to fulfill monitoring corrosion of reinforced concrete structures such as electrochemical methods, cover thickness measurement, X-ray radiography measurement as well as visual inspection. Actually, steel corrosion was electrochemical in nature, it was appropriate to monitor the development of steel conditions by means of electrochemical techniques such as HCP technique[5,6], linear polarization (LP) technique[7] and electrochemical impedance spectroscopy (EIS) technique[8-10]. Both the pitting potential ($E_p$) and the polarization resistance ($R_p$) of steel could be obtained by means of the analysis of the LP curve. However, compared to these electrochemical techniques, EIS technique was proved to be an useful tool to monitor the corrosion process of reinforced steel in concrete[11-14].

Traditional investigation of corrosion condition of reinforced steel in concrete structure by means of electrochemical techniques was performed through external sensors[8,12,15-17]. It was hard to obtain accurate results about the corrosion parameters of reinforced steel in concrete due to these difficulties such as liquid junction potential and high impedance of concrete between steel and RE. Therefore, embedded sensors were quite useful in corrosion monitoring of reinforced steel in concrete structures. A lot of research has been devoted to investigating the steel corrosion by means of embedded reference electrodes. Wei[18] has placed a $Cu/CuSO_4$ RE into concrete to study the development of the steel corrosion in concrete under the alternated drying/wetting corrosion environment. Karthick[19] embedded a $MnO_2$ RE in concrete to investigate these corrosion parameters concerning steel in concrete with 0 and 3% NaCl by weight of cement representing the passive and active conditions of steel respectively. However, the $Cu/CuSO_4$ RE exhibited poor stability and reliability, meanwhile, the $MnO_2$ RE did not belong to the traditional categories of REs because of the reason that the potential could not be described by any reversible thermodynamic reaction[20,21]. The improved Ag/AgCl RE has shown well performance in concrete environments, which seemed to be the most steady and reliable RE applied in concrete structure to monitor the corrosion condition of steel[20]. Besides, the concrete media between the reference electrode and steel reinforcement indicated high resistance and inhomogeneous characteristics[22-26], which had significant influence on the measurement accuracy of corrosion parameters of steel in concrete. In addition, the interference changed with the development of the distance between the steel and the reference electrode. Therefore, it was necessary to investigate the effect of concrete media on the corrosion monitoring of reinforced steel through embedded sensors. Apart from corrosion parameters of steel measured by these electrochemical techniques, the evolution of surface morphology of steel should also be characterized. Scanning electron microscope (SEM) was widely applied to observe the plane morphology of steel surface[15,27-30]. However, the accumulation of corrosion product would cause the obvious change of the roughness of steel surface. 3-dimensional (3D) digital video microscope could present the stereoscopic morphology image as well as 3D profile of steel surface. Which was very effective in investigation of the development of steel surface suffering from corrosion in concrete.

In our work, the evolution of steel corrosion in concrete under the accelerated drying/wetting cycle was monitored through embedded corrosion monitoring systems by means of electrochemical techniques. Meanwhile, the distance between the steel and the system ranging from 1 cm to 3 cm was taken into account as to investigate the influence of the distance on the measurement. Besides, 3-

dimensional (3D) surface morphology of embedded steel was detected through the 3D digital video microscope.


## 2. EXPERIMENT

### 2.1. Materials

The materials used in our work were No. 42.5 Ordinary Portland Cement (OPC). The oxide composition of OPC was presented in Table 1. All chemical reagents used in our study were analytical reagent grade.


**Table 1.** Chemical composition of OPC used in our work (%).

|      | $SiO_2$ | $Al_2O_3$ | CaO | $Fe_2O_3$ | MgO | $K_2O$ | $Na_2O$ | $SO_3$ | Ignition loss |
|------|---------|-----------|-------|-----------|------|--------|---------|--------|---------------|
| OPC  | 22.55   | 9.35      | 61.30 | 3.10      | 1.35 | 1.03   | 0.15    | 0.99   | 0.16          |


### 2.2. Mixture proportions and specimen preparation

This experimental was investigated with water to cement (w/c) ratio of 0.55. The designed mix of 336 : 185 : 657.7 : 1221.3 (cement : water : fine aggregate : coarse aggregate ) was used. All concrete specimens were cast in plastic mould with a size of 10cm ×10cm ×10cm.
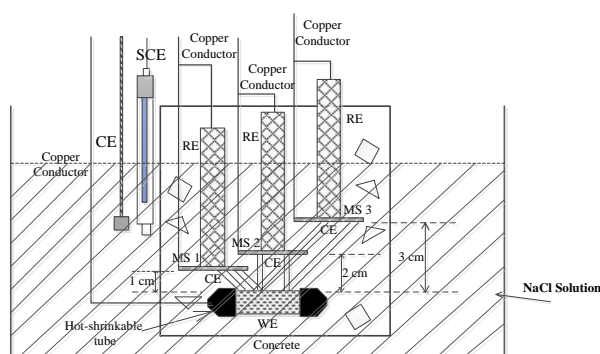


**Figure 1.** The diagram of concrete specimen with three sets of embedded corrosion monitoring systems assembled by (a) WE: working electrode, (b) RE: Ag/AgCl reference electrode and (c) CE: counter electrode. The external system consists of SCE (worked as CE) and square Pt electrode (worked as CE).


An carbon steel (1 cm in diam.) was placed in the concrete with three sets of corrosion monitoring systems consisted of a Ag/AgCl RE as well as a square Ti electrode with a size of 3cm × 3cm. But the distance between the monitoring system and the steel was set as 1cm, 2cm and 3cm, respectively. In this situation, MS 1, MS 2 and MS 3 were applied to denote these three embedded corrosion monitoring systems. The fabrication procedure of this improved Ag/AgCl RE has been

described in detail in literature[20]. The external monitoring system was made up from a saturated calomel electrode (SCE) and a square Pt electrode. Besides, the exposed length of the embedded steel was ca. 2 cm and the chemical composition (in wt%) was 0.22 C, 0.30 Si, 0.65 Mn, 0.05 S, 0.045 P and the residual Fe. The scheme of the concrete sample was presented in Fig. 1.

After the concrete specimens have been stored in a 95% humidity chamber at 20±2℃ for 28 d. These specimens were carried out with accelerated drying/wetting cycles. At first the specimen was performed in an exposure of 3 days under the room temperature, after that, immersed in 5 wt % NaCl solution for 4 days. Thus, the cyclic period was one week. The total testing time for the drying/wetting cycles was 20 cycles. To simplify the description, C1, C2, C4, C6, C9, C14 and C20 were used to refer to the 1, 2, 4, 6, 9, 14 and 20 drying/wetting cycles.

## 2.3. Corrosion conditions of steel investigated by embedded and external monitoring systems

All the electrochemical tests were conducted with a Princeton Applied Research (PAR) STAT 2273 Potentiostat. If not specified, these experiments were executed at room temperature (25°C).

### 2.3.1. Linear polarization measurements

LP tests of steels were carried out with respect to these embedded corrosion monitoring systems, meanwhile, the same tests were performed by the external system after several cycles. LP scan was performed between -20 mV and 20 mV with respect to open circuit potential at a sweep rate of 0.166 mV/s. Moreover, the polarization resistance ($R_p$) obtained according to LP curve was introduced into the Stern-Geary equation to calculate the corrosion rate. This Stern-Geary equation is

$$I_{corr} = \frac{B}{R_p} \qquad (1)$$

where, B is the Stern-Geary constant. The value of 26 mV was adopted for active steel and 52 mV for passive steel[31].

### 2.3.2. Electrochemical impedance spectra measurements

Similar to the LP tests, the EIS measurements for steel were also carried out with respect to embedded and external corrosion monitoring systems, respectively. In addition, the frequency ranged from 10 mHz to 1 MHz was performed in the EIS test. And the EIS results were analyzed by means of the ZSimpWin software based on these equivalent circuit models. The $I_{corr}$ was also calculated by the Stern-Geary equation presented in Eq. (1) based on the $R_p$ obtained by EIS measurement.

### 2.3.3. Half-cell potential measurements

The half-cell potential of steel was monitored periodically with respect to these embedded and external monitoring systems, respectively. And the passive/active potential of steel could be confirmed based on the $i_{corr}$ values obtained from LP and EIS tests.

*2.4. Morphology observation*

        The surface morphology of the steel embedded in concrete after the accelerated drying/wetting cycles of 4, 8, 13 and 20 was observed by a HIROX KH-7700 3D digital video microscope (Hirox Co. LTD, Japan). This microscope applied a composite of multiple images through different focal planes to construct a 3-dimensional (3D) profile by which cross-sectional profile and height data could be obtained.


## 3. RESULTS AND DISCUSSION

*3.1. Corrosion monitoring of steels by embedded and external electrodes*

*3.1.1. Linear polarization measurements of steel*
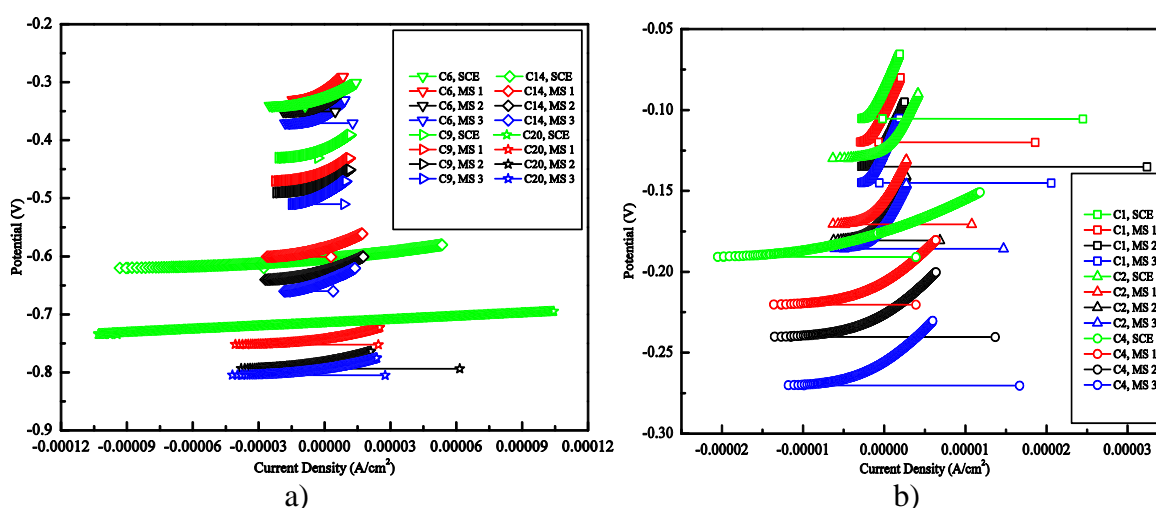


**Figure 2.** Linear polarization curves for steel in concrete specimens measured by embedded and external monitoring systems with the sweep rate of 0.166 mV/s: (a) cycle 1, 2 and 4, (b) cycle 6, 9, 14 and 20. MS and SCE represent embedded and external systems, respectively.


        Fig. 2 shows the linear polarization (LP) plots for the steel in concrete investigated by embedded and external monitoring systems with different drying/wetting cycles. It could be clearly seen form Fig. 2 that steel potential became more negative with the development of drying/wetting cycles. Besides, the slope of the LP plot also dropped with the increase of the cycles. At the beginning of the test, the steel kept the passive state, therefore, the slope value of the plot was in high level. However, a sharp decrease of the slope of plot after cycle 4 has been observed due to the pitting corrosion of steel initiated. After that, the slope of the curve decreased quickly with the accelerated corrosion cycles. So far, the LP technique has become a widely used way of measuring the instantaneous corrosion condition of reinforced steel embedded in concrete[32,33]. In addition, this technique was non-destructive and rapid, causing only little damage to the concrete cover to prompt an electrical connection to be fulfilled to the rebar. Therefore, LP technique has been widely applied

either in laboratory or field to obtain the accurate corrosion parameters concerning the steel in concrete. The LP technique was at first proposed based on the Stern-Geary theory[34] in which the corrosion current, $I_{corr}$, was given by

$$I_{corr} = \frac{\beta_a \beta_c}{2.3(\beta_a + \beta_c)} \frac{1}{R_{ct}} = \frac{B}{R_{ct}} \qquad (2)$$

where, $B$ was the Stern-Geary constant, $R_{ct}$ was the charge transfer resistance, and $\beta_a$ as well as $\beta_c$ were anodic and cathodic Tafel constants, respectively. The value of the Stern-Geary constant, B, usually ranged from 12 to 52 mV in the situation of steel reinforcement investigation. Generally, higher corrosion condition led to lower obtained values for the Stern-Geary constant. For conditions where it was almost impossible to calculate the constant because of the destructive feature of the investigation, therefore, it was recommended that the B value of 26 mV and 52 mV were applied as an averaged value for the steel under the active and passive condition respectively in order to reduce the error for calculating this parameter.

For the purpose of obtaining the polarization resistance ($R_p$), a small amount around the equilibrium potential was applied to the steel. Which could be carried out potentiostatically by means of changing the steel potential according to a fixed value, $\Delta E$, and recording the current decay, $\Delta I$, after a fixed period. On the other hand, it could also be performed galvanostatically by putting on a small constant current, $\Delta I$, to the reinforced steel and measuring the development of the potential, $\Delta E$, after a fixed time. Hence, the change in steel potential, $\Delta E$, fallen in the linear Stern–Geary range of 10-40 mV was chosen in each situation. The $R_p$ value of the steel was then calculated based on this formula:

$$R_p = \frac{\Delta E}{\Delta I} \qquad (3)$$

Then the corrosion rate, $I_{corr}$, could be obtained according to Eq. (1) based on the $R_p$ value calculated from Eq. (3).
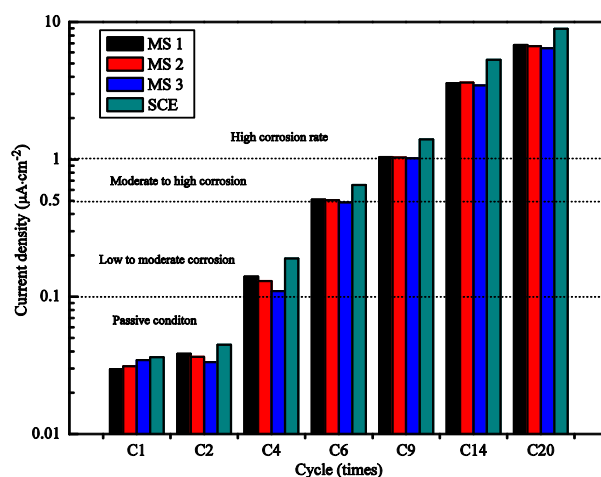


**Figure 3.** The development of corrosion current densities of steels in concrete specimens with drying/wetting cycles obtained by linear polarization technique through embedded and external monitoring systems. MS and SCE represent embedded and external systems, respectively.

However, the value of corrosion rate of steel was dependent on the surface area of the steel (i.e., the exposed surface). Therefore, it was accurate to determine the corrosion state of steel by means of corrosion current density, $i_{corr}$. In order to obtain the $i_{corr}$ value, the surface area, A, of steel which has been polarized needed to be precisely known:

$$i_{corr} = \frac{I_{corr}}{A} \qquad (4)$$

Fig. 3 indicates the evolution of $i_{corr}$ value of steel in concrete with the drying/wetting cycles according to the LP results. According to these literatures[4,35,36], the steel in concrete was under passive condition when the $i_{corr}$ value was lower than 0.1 $\mu A \cdot cm^{-2}$. And the steel exhibited a high corrosion rate condition in the case that the $i_{corr}$ value exceeded 1 $\mu A \cdot cm^{-2}$. Besides, the steel was in the moderate to high corrosion condition when the $i_{corr}$ value ranged between 0.5 and 1$\mu A \cdot cm^{-2}$. At the beginning of the accelerated test (C1 and C2), the $i_{corr}$ value of steel was obviously lower than 0.1$\mu A \cdot cm^{-2}$, which proved that the steel was under the passive condition. The difference between the corrosion current density of steel under passive state obtained by the external and embedded monitoring systems could be neglected. The $i_{corr}$ value exceeded 0.1$\mu A \cdot cm^{-2}$ after cycle 4, indicating that the corrosion of steel has been initiated. Moreover, the $i_{corr}$ value increased quickly once the corrosion has been induced. Hence, the steel was in low to moderate corrosion condition during the process of cycle 4 to cycle 6. However, the $i_{corr}$ value of steel after cycle 9 was as high as 0.8$\mu A \cdot cm^{-2}$, which demonstrated that the steel has been located in moderate to high corrosion condition. Then the steel was under high corrosion rate state after cycle 14. The $i_{corr}$ value of steel in corrosion condition monitored by MS 2 was a little higher than that by MS 1. Nevertheless, the value obtained by MS 3 was obviously lower than these measured by MS 1 and MS 2. Since the distance between MS 3 and steel has reached 3 cm, the high concrete resistance and the heterogeneity of the concrete structure produced significant influence on the measurement. Based on our foundation, the distance between the corrosion monitoring system and steel should not exceed 2 cm.

It was necessary to place the corrosion monitoring system near the working electrode as soon as possible for the purpose of obtaining accurate information about the steel condition. In addition, the corrosion current density of reinforced steel in concrete structure investigated by external SCE was obviously in higher level compared to that by these embedded electrodes. Which confirmed that the corrosion rate of steel in concrete was in higher side with respect to external monitoring system when compared to the embedded one. The similar foundations have also been presented by Karthick and Muralidharan[19,22]. The difference between the corrosion current density obtained by the external electrode and the embedded one seemed to be larger with the development of the drying/wetting cycles. Thus, the corrosion condition of steel determined according to the results measured by the external SCE was much heavier than the actual state of steel. Therefore, based on the above investigation, for the use of life prediction of field concrete structures, accurate measurements of corrosion state of steel was pre-requisite. In such situations the embedded corrosion rate monitoring system precisely predicted the change of the condition of steel in concrete.

*3.1.2. Electrochemical impedance spectra measurements of steel*

Fig. 4 depicts the Nyquist plots of steel in concrete after different cycles of the accelerat ed drying/wetting corrosion test. Generally, Nyquist curves indicate a capacitive loop of depressed semicircles. In addition, as the increase of the testing time, the diameter of semicircle was gradually reduced, which was ascribed to the reason that the erosion of chloride ions on the passive film on the sample surface.
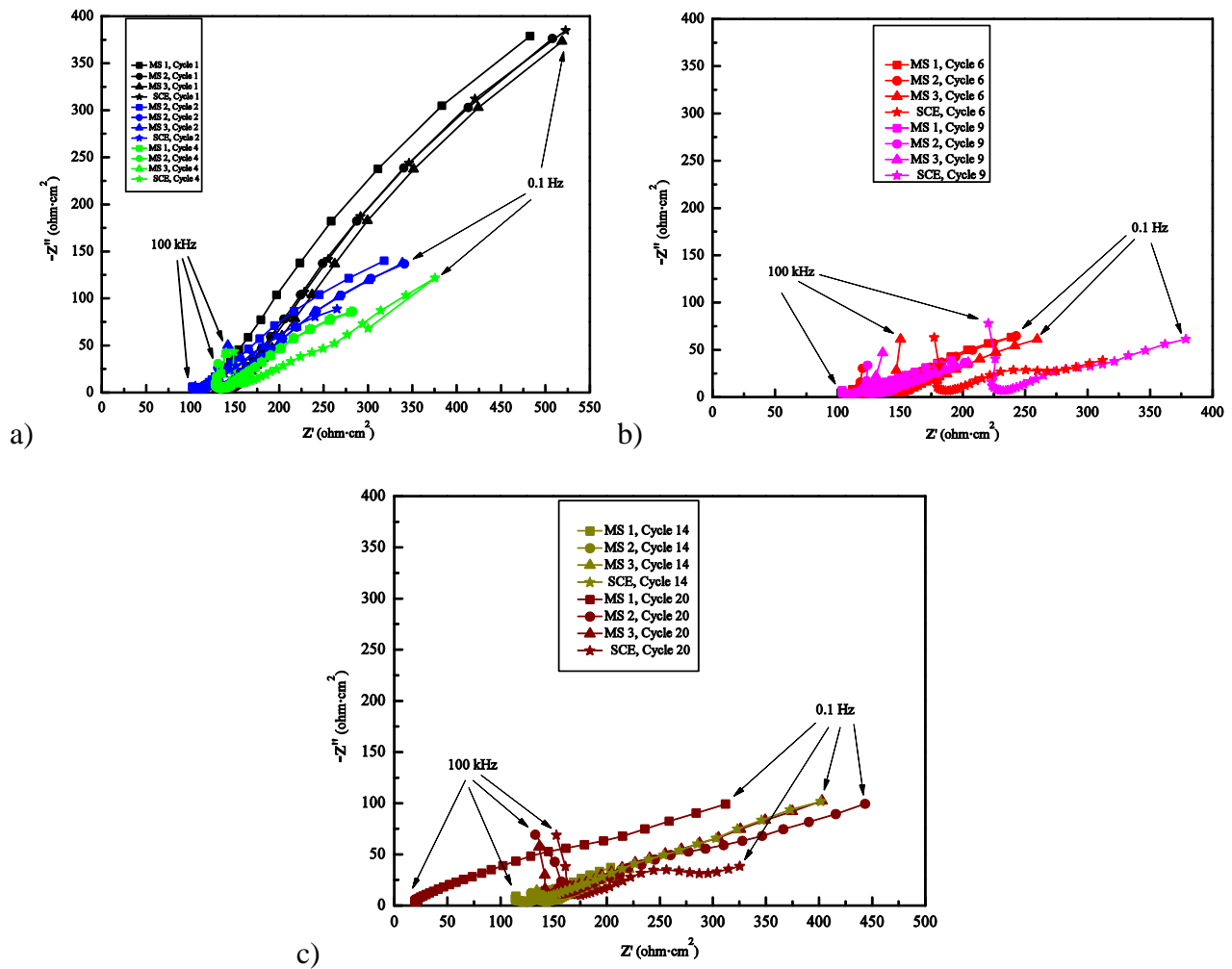


**Figure 4.** The development of Nyquist plots of steel in concrete specimens with drying/wetting cycles obtained by EIS technique with the applied frequency ranged from 10 mHz to 1 MHz through embedded and external monitoring systems: (a) cycle 1, 2 and 4, (b) cycle 6 and 9, (c) cycle 14 and 20. MS and SCE represent embedded and external systems, respectively.

However, in contrast to the LP technique, the accuracy of the results measured by EIS was based on the use of equivalent-circuit model (ECM). The complex impedance plot comprised two distinct arcs in high and low frequency, which were associated with bulk concrete response and steel surface response, respectively[7]. Therefore, an appropriate ECM should be introduced to analyze the

Nyquist plots. The ECM used in our investigation comprised three time constants in series with the electrolyte resistance, i.e., the Randles circuit, shown in Fig. 5.
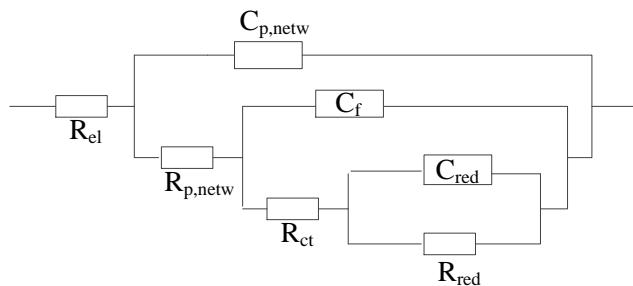


**Figure 5.** Equivalent electrical circuit for the reinforcement concrete system.

This model has been introduced in this literature[37] to fit the EIS results of steel embedded in concrete. In this model, the $R_{el}$ was the concrete resistance dealing with the contribution of the electrolyte resistance in the situation of measurements in concrete. The first time constant ($R_{p,netw}$, $C_{p,netw}$) was ascribed to the characteristics of concrete based on pore network. And the second time constant ($R_{ct}$, $C_f$) involved the electrochemical reaction produced on rebar surface. The third time constant ($R_{red}$, $C_{red}$) was attributed to redox process, happening in the productive layers. As a rule, the scope of high-frequency in the plots indicates the information of the electrolytic solution resistance and the interface resistance between the steel and electrolytic solution, nevertheless, the range of low frequency depicts the charge transfer resistance, which is equivalent to the polarization resistance ($R_P$). Thus, for deriving $R_P$ from EIS results, the low frequency region (7.27 Hz to 0.1 Hz) in the impedance spectra was usually considered for calculations. Thus, the fitting result parameters calculated from the EIS plots based on the Randles circuit have been presented in Table 2.
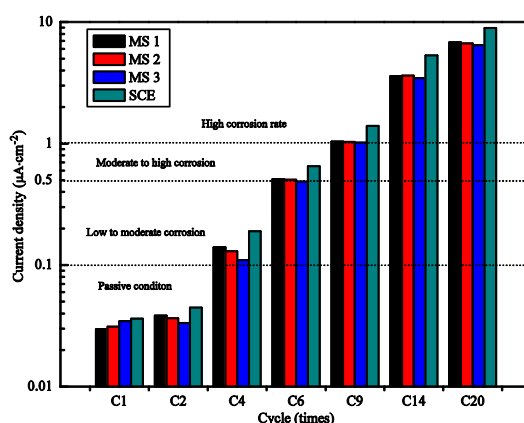


**Figure 6.** The development of corrosion current densities of steels in concrete specimens with drying/wetting cycles obtained by EIS technique through embedded and external monitoring systems. MS and SCE represent embedded and external systems, respectively.

It was necessary to calculate the value of $R_P$ in order to obtain the $i_{corr}$ value of the steel. $R_P$ value was same to that of $R_{ct}$ in the case that the test was performed in the simulating concrete solutions or cement extract solutions[7,8,16,38]. Besides, $R_P$ value equaled $R_{ct}$ in this situation that there were no mass transport limitations. However, intermediate layer would experience the process of transformations (contributions of the product layer) when absorbed. Therefore, the $R_P$ value could be obtained by means of adding $R_{ct}$ to $R_{red}$ which referred to the process of redox transformations as well as mass transfer[39]. Moreover, the calculated $R_P$ value was introduced to Eq. (1) in order to obtain the value of $I_{corr}$. Then the $i_{corr}$ value could be obtained according to Eq. (4).

**Table 2.** Fit parameters from experimental EIS results of the steel in concrete measured by different monitoring systems.

| Cycle | Monitoring system | $R_{el}$ (k$\Omega$·cm$^2$) | $C_{p, netw}$ (10$^{-3}$μF/cm$^2$) | $R_{p, netw}$ (k$\Omega$·cm$^2$) | $C_f$ (μF/cm$^2$) | $R_{ct}$ (k$\Omega$·cm$^2$) | $C_{red}$ (μF/cm$^2$) | $R_{red}$ (k$\Omega$·cm$^2$) |
|---|---|---|---|---|---|---|---|---|
| 1 | MSE 1 | 55.01 | 6.53 | 39.23 | 45.82 | 98.14 | 57.11 | 87.07 |
| | MSS 2 | 53.01 | 7.08 | 44.95 | 48.54 | 86.09 | 58.10 | 91.08 |
| | MSE 3 | 51.52 | 7.51 | 47.31 | 53.55 | 78.21 | 47.51 | 81.34 |
| | SCE | 34.11 | 3.09 | 33.58 | 63.12 | 73.09 | 65.09 | 78.73 |
| 2 | MSE 1 | 37.21 | 6.81 | 35.12 | 85.13 | 75.54 | 76.09 | 68.90 |
| | MSE 2 | 33.43 | 7.56 | 33.12 | 81.09 | 77.23 | 73.31 | 74.30 |
| | MSE 3 | 29.82 | 8.35 | 41.73 | 73.07 | 86.16 | 64.03 | 79.12 |
| | SCE | 45.02 | 4.71 | 37.10 | 95.04 | 64.05 | 87.11 | 59.13 |
| 4 | MSE 1 | 28.15 | 7.15 | 17.05 | 123 | 9.13 | 178 | 10.57 |
| | MSE 2 | 25.71 | 6.92 | 15.14 | 119 | 9.89 | 179 | 11.33 |
| | MSE 3 | 20.13 | 7.81 | 11.73 | 115 | 11.23 | 183 | 13.85 |
| | SCE | 18.73 | 5.10 | 14.52 | 118 | 6.94 | 163 | 7.58 |
| 6 | MSE 1 | 17.97 | 8.03 | 13.65 | 159 | 2.51 | 245 | 2.90 |
| | MSE 2 | 15.49 | 8.51 | 11.35 | 153 | 2.73 | 251 | 2.95 |
| | MSE 3 | 11.23 | 7.98 | 10.37 | 163 | 2.54 | 258 | 3.15 |
| | SCE | 9.58 | 9.35 | 13.57 | 139 | 1.94 | 215 | 2.30 |
| 9 | MSE 1 | 9.51 | 7.89 | 5.89 | 215 | 1.20 | 289 | 1.45 |
| | MSE 2 | 9.03 | 8.90 | 4.89 | 208 | 1.19 | 295 | 1.51 |
| | MSE 3 | 7.53 | 9.10 | 4.12 | 196 | 1.31 | 317 | 1.39 |
| | SCE | 14.32 | 12.51 | 7.81 | 183 | 0.72 | 291 | 1.25 |
| 14 | MSE 1 | 5.72 | 9.11 | 3.81 | 270 | 0.28 | 335 | 0.49 |
| | MSE 2 | 5.11 | 9.78 | 3.05 | 267 | 0.29 | 351 | 0.47 |
| | MSE 3 | 4.87 | 9.91 | 2.79 | 249 | 0.35 | 377 | 0.45 |
| | SCE | 4.11 | 8.71 | 2.53 | 257 | 0.13 | 411 | 0.39 |
| 20 | MSE 1 | 3.79 | 10.30 | 2.57 | 350 | 0.12 | 475 | 0.29 |
| | MSE 2 | 3.41 | 12.41 | 2.17 | 337 | 0.14 | 491 | 0.27 |
| | MSE 3 | 3.07 | 12.53 | 1.89 | 313 | 0.18 | 513 | 0.25 |
| | SCE | 2.67 | 9.89 | 2.19 | 333 | 0.12 | 483 | 0.19 |

Fig. 6 indicates the change of $i_{corr}$ value of steel with the drying/wetting times obtained based on the EIS results. Generally, with the increase of the drying/wetting cycles, the $i_{corr}$ values of steel became larger. The corrosion condition of steel could be determined based on the $i_{corr}$ value of steel, which has been presented in Sect. 3.1.1. Thus, Fig. 6 clearly exhibited the steel was in passive state during the first two cycles. The corrosion of steel was initiated from the beginning of the cycle 4, i.e., the $i_{corr}$ of steel exceeded $0.1\mu A \cdot cm^{-2}$. Once the steel corrosion was initiated, the $i_{corr}$ increased rapidly with the development of the testing time. Which was attributed to the breakage of the protective layer, displaying the active corrosion of pitting happened. Hence, the steel was located in moderate to high corrosion rate after cycle 6. In addition, the corrosion current density of steel was higher than $1\mu A \cdot cm^{-2}$ in cycle 9, which proved that the steel lay in high corrosion rate condition.

Besides, during the period of the whole accelerating corrosion cycles, the corrosion current density of steel measured by MS 2 and 3 was slightly lower than that measured by MS 1 whether in passive or active conditions. Which was ascribed to the reason that the distance between the steel and monitoring system in concrete. However, the corrosion current density of steel investigated by the external monitoring system (SCE) was significantly greater than that measured by these embedded systems. As described by Karthick and Muralidharan[19], the corrosion current density of steel measured by the surface mounted monitoring system was about 25% higher than that measured by the embedded system. Based on our investigation, the corrosion current density monitored by the external SCE was 30% to 40 % higher than that by the embedded one. The large deviation in the corrosion current density between the external and embedded monitoring systems was attributed to the reason that concerning the liquid junction and IR drop problem generated in concrete environment due to the high resistance and the heterogeneity reported by Atkins[25] and Ueli[40-42]. Therefore, the evaluation of the steel condition based on the investigation by the embedded monitoring system was more accurate compared to that measured by external system.
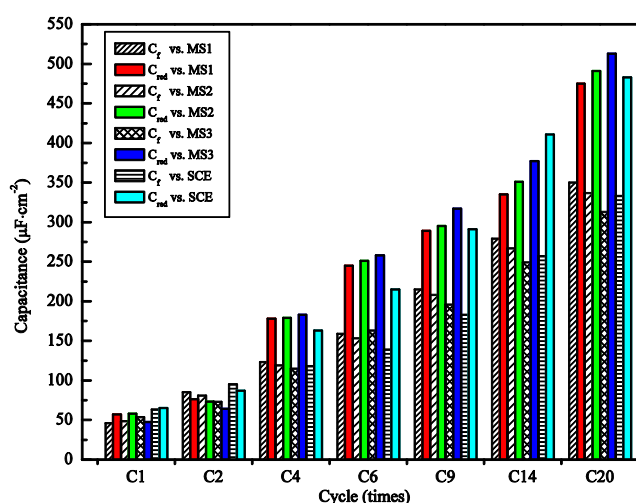


**Figure 7.** The development of $C_f$ and $C_{red}$ of steel in concrete specimens with drying/wetting cycles obtained by EIS technique through embedded and external monitoring systems. MS and SCE represent embedded and external systems, respectively.

Fig. 7 indicates the evolution of the interfacial capacitance $C_f$ as well as the capacitance $C_{red}$ with the drying/wetting cycles. Generally, with the increase of the drying/wetting cycle, both $C_f$ and $C_{red}$ became larger, especially when the corrosion of steel has been initiated. According to Bataillon and Brunet[43], the $C_f$ was determined by Helmholtz model, presented by Eq. (5):

$$C_f = \frac{\varepsilon \varepsilon_o A}{d} \qquad (5)$$

in which $\varepsilon$ was the dielectric constant of the medium, $\varepsilon_o$ the vacuum permittivity as well as $d$ was the thickness of the layer generated on the steel surface, besides, $A$ was the effective surface area of the steel. Thus, when the harmful ion ($Cl^-$) intruded into the steel/concrete interface, the thickness of the protective layer would be decreased quickly because of the local damage of the protective film. Therefore, the $C_f$ of steel increased significantly once the corrosion has been initiated. Except cycle 1, the $C_f$ value of steel measured by the embedded monitoring system dropped with the increase of the distance between the steel and the system. Which was ascribed to the reason that the heterogeneous concrete media had great influence on the current flow between the working electrode and the counter electrode as well as the response of the reference electrode to the working one. As for the steel under passive state (cycle 1 and cycle 2), the value of $C_{red}$ was close to that of $C_f$ (lower than 100 $\mu F/cm^2$), which was similar to that reported by Koleva[37]. As for the steel in low to moderate corrosion rate and moderate to high corrosion rate conditions, the $C_f$ values were ca. 125 and 150 $\mu F/cm^2$, respectively. And the $C_f$ value exceeded 200$\mu F/cm^2$ when the steel was under high corrosion rate state. However, when steel was under active condition, the obtained $C_{red}$ values were significantly higher (presented in Fig.7) than that of $C_f$. Once the corrosion of steel was triggered, the $C_{red}$ of steel developed quickly for the reason that high rate of oxidation process happened in the layer generated on the rebar surface which was under the active state. The $C_{red}$ value of steel measured by MS 1 was clearly lower than that determined by MS 2 and MS 3. However, $C_f$ value of steel measured with respect to MS 1was in higher side compared to that measured by MS 2 and MS 3. Based on this, there was relatively large difference between the capacitance determined by MS 1 and that by MS 2 or MS 3. Therefore, the capacitance of steel obtained by MS 1 was more accurate than those measured with respect to others.
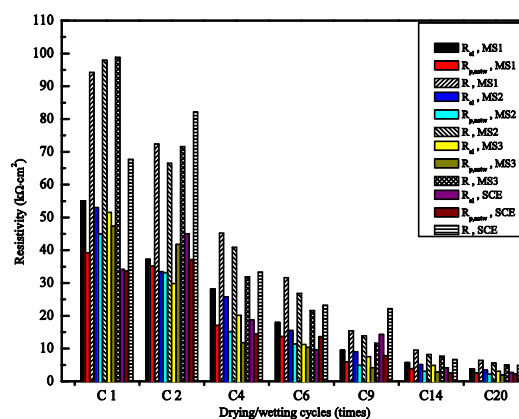


**Figure 8.** The development of $R_{el}$, $R_{p,netw}$ and $R$ of steel in concrete specimens with drying/wetting cycles obtained by EIS technique through embedded and external monitoring systems. MS and SCE represent embedded and external systems, respectively.

Fig. 8 exhibits the evolution of concrete electrical resistivity (R) with the drying/wetting cycles, derived from EIS ($R_{el}$ + $R_{p,netw}$) plots. Generally, both $R_{el}$ and $R_{p, netw}$ of concrete dropped with the increase of the drying/wetting cycles. At the beginning of investigation, the $R_{el}$ value of concrete exceeded 55 kΩ·cm$^2$ and the $R_{p, netw}$ value was as high as 40 kΩ·cm$^2$. However, as the development of accelerated drying/wetting cycles, the $R_{el}$ value was reduced to ca. 10 kΩ·cm$^2$, meanwhile, the $R_{p, netw}$ was lower than 5 kΩ·cm$^2$. Though concrete hydration had a significant impact on the concrete resistivity, more important contributing factors were related to the environmental as well as technical conditions. The sustained invasion of chloride ions into the concrete during the period of drying/wetting cycles, which led to the continuous increase of chloride ion content in the pore solution of concrete. Therefore, concrete resistivity dropped quickly with the development of drying/wetting cycles. It should be pointed out that the resistivity measured by MS 1 was obviously higher than that measured through MS 2 or MS 3. Which was ascribed to the reason that the closer from the exposed faces, the higher the chloride ion concentration of concrete pore solution was. In addition, it was widely known that $C_3A$ and $C_4AF$ phases presented into concrete would bind $Cl^-$ to produce $3CaO·Al_2O_3·CaCl_2·10H_2O$ (i.e., Friedel's salt) and $3CaO·Fe_2O_3·CaCl_2·10H_2O$, repectively[44]. Besides, part of $Cl^-$ was adsorbed on the calcium silicate hydrates (C-S-H) and the other was still existed in the pore solution. Which led to the change of the composition as well as the microstructure of concrete structure. In this situation, the dielectric constant of the medium would increase significantly. Which also contributed to the increase of the value of $C_f$ in the progress of the drying/wetting cycles. Besides, due to the SCE placed in the external solution, the accuracy of concrete resistivity measured by the external electrode was poor.

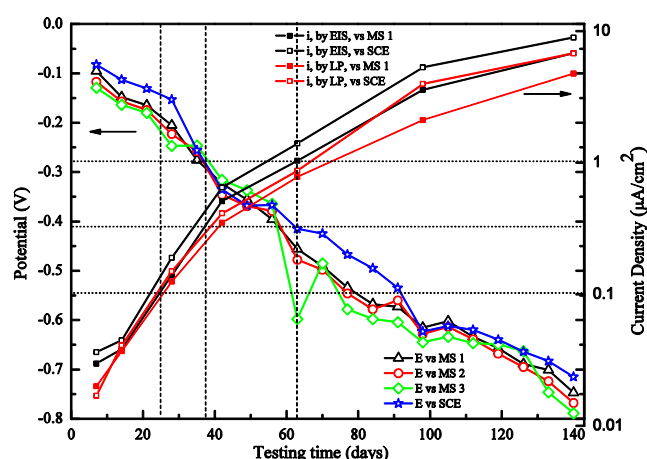### 3.1.3. Half-cell potential measurements of steel



**Figure 9.** The change of half-cell potential and corrosion current density of steel with the testing time measured through embedded and external monitoring systems. MS and SCE represent embedded and external systems, respectively.

In Fig. 9, the evolution of half-cell potential of steel in concrete investigated with respect to embedded and external monitoring systems has been indicated. The development of corrosion current density ($i_{corr}$) of steel monitored through embedded MS 1 and external SCE by means of LP and EIS techniques has also been presented in this figure. It should be pointed out that the $i_{corr}$ value of steel characterized by LP technique was obviously lower than that measured by EIS technique. According to Law[45], the polarization resistance ($R_p$) determined by LP technique included the charge transfer resistance ($R_{ct}$) as well as the solution resistance ($R_s$), namely the formula below:

$$R_p = R_{ct} + R_s \qquad\qquad (6)$$

Actually, the $R_p$ value of steel obtained through LP technique presented in the Sect 3.1.1 was inconsistent with the value calculated by adding the $R_{ct}$ value and $R_s$ value determined by means of the EIS technique. Nevertheless, the polarization resistance determined by LP technique was significantly larger than that by EIS technique. Based on this, the corrosion current density of steel obtained through LP method was obviously lower than that by EIS technique. From the above analysis it was clearly proved that the corrosion rate of steel in concrete was always in lower side with respect to the LP technique when compared to the EIS technique. Therefore, the corrosion rate of steel in concrete was determined based on the corrosion current density measured by means of the EIS technique. Besides, as presented in Sect 3.1.2, the corrosion rate of steel in concrete obtained by embedded electrode was more accurate compared to that by external one. Hence, the corrosion condition of steel was confirmed based on the corrosion current density obtained by EIS technique through MS 1.

Thus, the half-cell potential (HCP) of steel was higher than -185 mV with respect to MS 1 when the steel was under the passive condition. And the HCP of steel in the low to moderate corrosion rate condition lay between -185 and -297 mV with respect to MS 1. Moreover, the potential of steel in the moderate to high corrosion rate condition was between -297 and -455 mV vs. MS 1. Besides, the HCP of steel under high corrosion rate condition was more negative than -455 mV vs. MS 1. It was observed that the embedded corrosion monitoring system could clearly distinguish these different conditions of steel in concrete. This behavior was quit suitable for our interest to apply the embedded monitoring system in corrosion investigation of steel in concrete.

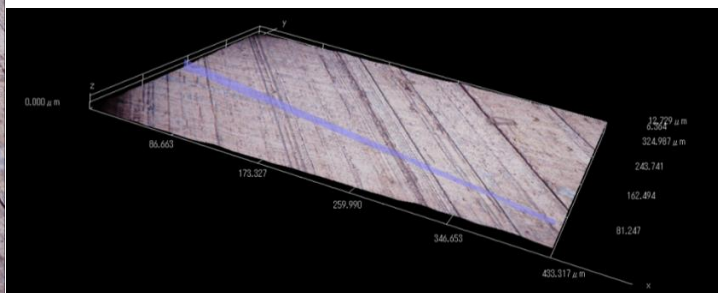## 3.2. Morphology observation

By means of the 3D digital microscope, the morphologies of the surfaces of steel in different testing periods were further analyzed. Fig. 10 indicates the surface and the 3-dimensional (3D) morphology as well as the 3D profile images of steel after various accelerated cycles. Fig. 10a shows the surface morphology of steel after cycle 4 was still smooth and little rust spots have been detected even though the corrosion current density determined by EIS technique has exceeded $0.1\mu A\cdot cm^{-2}$ which proved that the corrosion has been initiated. According to the 3-D morphology (Fig. 10b), the maximum height difference (MHD), i.e., the height presented in the profile image (Fig. 10c), was only about 8.6 μm. Which in turn suggested that the surface of steel was smooth. The surface morphology of steel after cycle 8 has been presented in Fig. 10d. The majority of the steel surface was still smooth and brilliant. However, a little yellow and localized as well as scattered rust spots have been detected

on the surface of steel. Actually the corrosion state of steel in concrete after C8 characterized by electrochemical technique was almost in heavy corrosion condition along with a high corrosion rate. At the same time, the MHD of the 3-D morphology of steel surface after C8 was ca. 10μm which was close to that of steel after C4. Although the corrosion rate of steel indicated a clearly increase with the development of accelerated drying/wetting cycles, slow accumulation of corrosion products of steel in concrete has been found out which was ascribed to the reason that the high alkaline environment in concrete would produce an pronounced protective effect on steel subjected to the chloride ion attack. Besides, a large amount of dispersed rust spots have been determined on the surface of steel after C13 (Fig. 10g) compared to that after C8. Nevertheless, there was still no significant accumulation of corrosion products on the surface of reinforced steel. Which could also be certified by the characterization of the 3-D morphology of steel that the MHD of steel after C13 was only 1.2μm higher than that after C8. The height variation of steel surface was still ascribed to the reason that the rebar surface was polished vigorously in the process of pretreatment. The accumulation of corrosion product had little influence on the height difference of the surface morphology of steel. The morphology of steel after C20 has been presented in Fig. 10j from which a large area of continuous rust region has been detected compared to the "dotted" rust spots determined in the previous analyzes. Based on the 3-D morphology of steel surface (Fig. 10k), the obvious accumulation of corrosion product has been presented in this photo which led to the significant increase of the height of rebar surface since that the MHD of surface was as high as 17.6μm according to the profile of 3-D morphology indicated in Fig. 10l. The height of surface after C20 was almost 8μm higher than that after C8.

Since the corrosion products generated as a consequence of the corrosion had a volume 2-4 times than that of rebar[46,47], which caused volume expansion leading to tensile stressed in concrete, leading to cracking as well as spalling of concrete. The generation of corrosion products not only caused damage to concrete but also led to the increase of height of steel surface. Therefore, the amount of corrosion products could be determined by means of the variation of the height of steel surface. The accurate evaluation of the condition of steel could be realized by means of the 3-D morphology which had these advantages such as visualization and quantitative calculation.
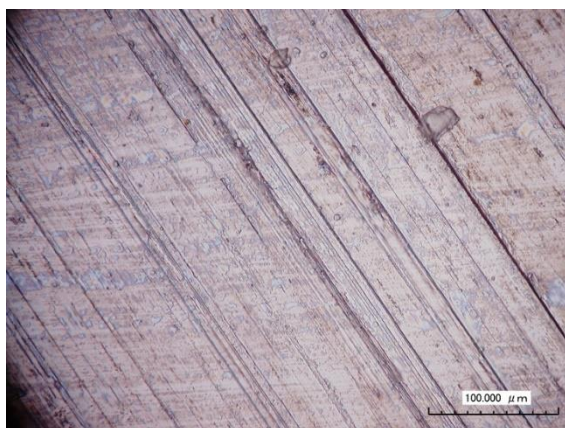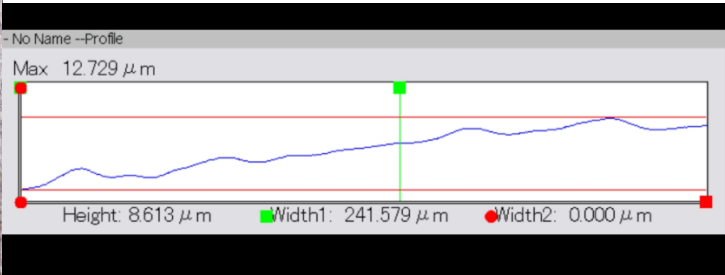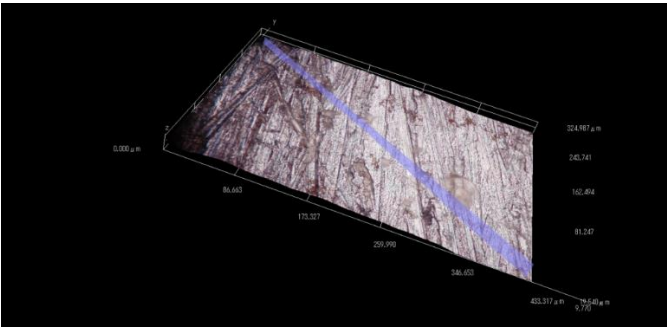


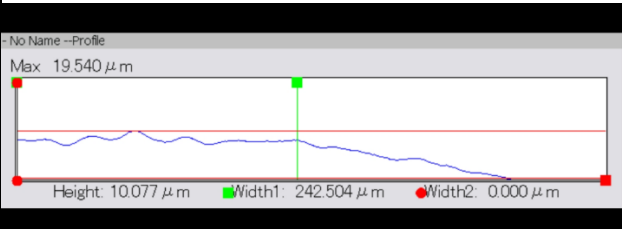(a) surface of steel after C4                                           (b) 3D morphology of steel after C4
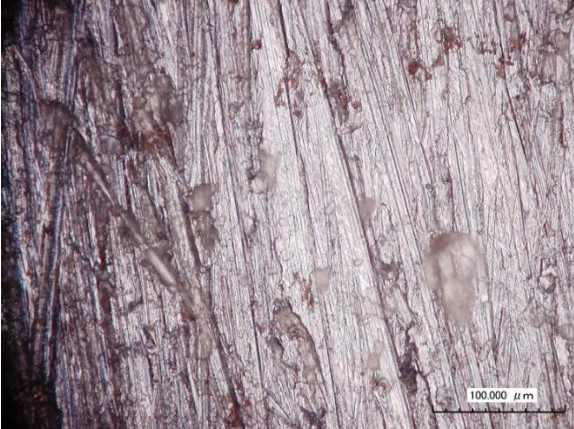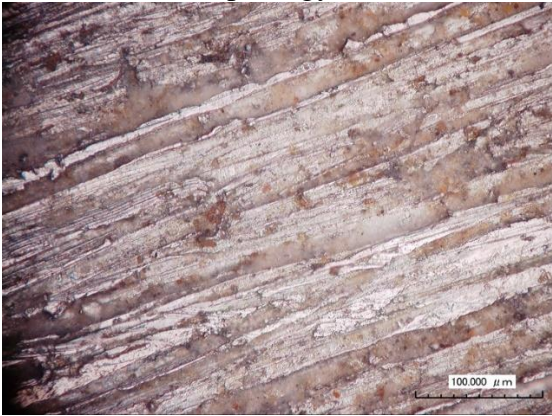
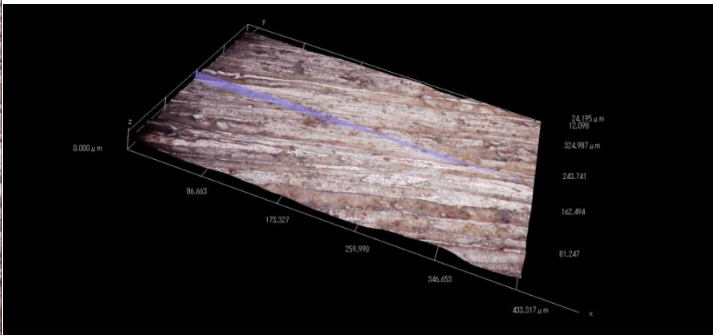(d) surface of steel after C8



(c) 3D profile of steel after C4



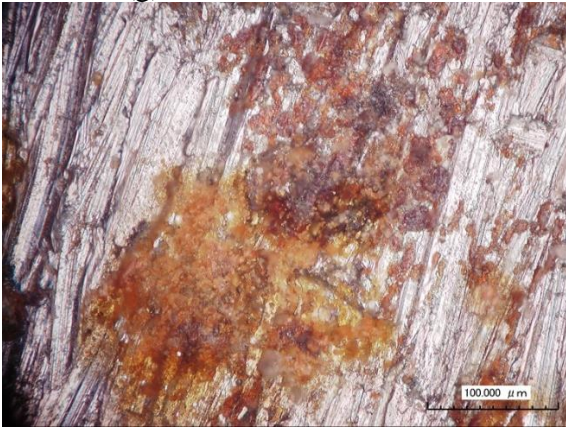(e) 3D morphology of steel after C8



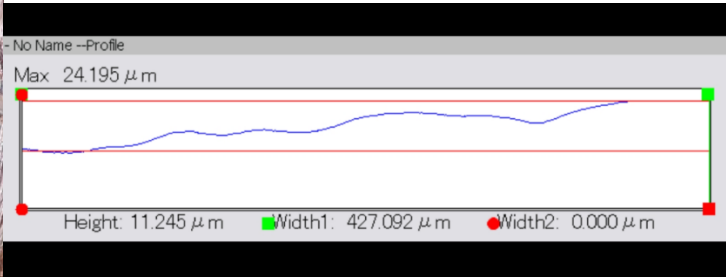(f) 3D profile of steel after C8



(g) surface of steel after C13
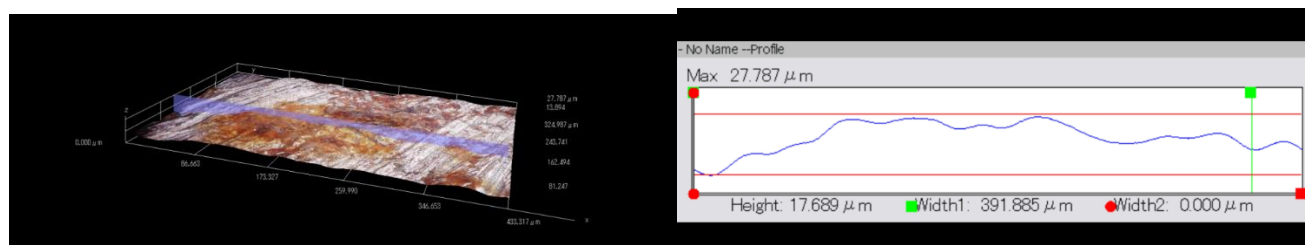


(h) 3D morphology of steel after C13



(j) surface of steel after C20



(i) 3D profile of steel after C13

(k) 3D morphology of steel after C20                    (l) 3D profile of steel after C20

**Figure10.** The development of surface, 3D morphology and 3D profile of steel with different drying/wetting cycles.

Hence, it was recommended to investigate the change of the state of steel surface subjected to corrosion attack by the 3-D morphology technique.

## 4. CONCLUSION

To sum up, in this investigation, the influence of the distance between the embedded corrosion monitoring system and the reinforced steel on the corrosion measurement in concrete has been investigated. Generally, the corrosion rate of steel determined by LP technique with respect to MS 3 was higher than that by MS 1. However, the corrosion rate obtained by EIS technique through MS 2 and 3 was lower than MS 1. Besides, the $C_{red}$ value measured by MS 1 was clearly lower than that determined by MS 2 and MS 3. But the $C_f$ value measured through MS 1was in higher side compared to that by MS 2 and MS 3. All the studies validated the corrosion parameter determined by MS 1 was more accurate than the others. Based on this, the half-cell potential (HCP) of steel in concrete with respect to MS 1 are -185, -185 to -297, -297 to -455 and -455 mV for passive, low to moderate corrosion rate, moderate to high corrosion rate and high corrosion rate conditions. It was recommended to place the corrosion monitoring system close to the working electrode as soon as possible in order to obtain the precise measurements of corrosion condition of steel.

The accurate evaluation of the condition of steel could be realized by means of the 3-D morphology technique due to the accumulation of corrosion products on the steel surface. Hence, it was also recommended to investigate the change of the state of steel surface subjected to corrosion attack by the 3-D morphology technique.

## References

1.  C. Sun, S. Liu, J. Niu and W. Xu, *Int. J. Electrochem. Sci.*, 10 (7) (2015) 5309-5326.
2.  O.A. Omotosho, C.A. Loto, O.O. Ajayi, J.O. Okeniyi and A.P.I. Popoola, *Int. J. Electrochem. Sci.*, 9 (4) (2014) 2171-2185.
3.  J.O. Okeniyi, C.A. Loto and A.P.I. Popoola, *Int. J. Electrochem. Sci.*, 10 (12) (2015) 9893-9906.
4.  H. Song and V. Saraswathy, *Int. J. Electrochem. Sci.*, 2 (2007) 1-28.
5.  B. Elsener, C. Andrade, J. Gulikers, R. Polder and M. Raupach, *Mater. Struct.*, 36 (261) (2003) 461-471.
6.  G.S. Duffó, S.B. Farina and C.M. Giordano, *Electrochim. Acta*, 54 (3) (2009) 1010-1020.
7.  J. Xu, L. Jiang and J. Wang, *Constr. Build. Mater.*, 23 (5) (2009) 1902-1908.
8.  C. Ye, R. Hu, S. Dong, X. Zhang, R. Hou, R. Du, C. Lin and J. Pan, *J. Electroanal. Chem.*, 688 (2013) 275-281.
9.  C.H. Hsu and F. Mansfeld, *Corrosion*, 57 (09) (2001).
10. C. Xiong, L. Jiang, Y. Zhang, H. Chu and P. Jiang, *Mater. Lett.*, 174 (2016) 234-237.
11. M. Ismail and M. Ohtsu, *Constr. Build. Mater.*, 20 (7) (2006) 458-469.
12. F. Zhang, J. Pan and C. Lin, *Corros. Sci.*, 51 (9) (2009) 2130-2138.
13. M. Serdar, C. Meral, M. Kunz, D. Bjegovic, H. Wenk and P.J.M. Monteiro, *Cem. Concr. Res.*, 71 (2015) 93-105.
14. D.V. Ribeiro and J.C.C. Abrantes, *Constr. Build. Mater.*, 111 (2016) 98-104.
15. F. Zhang, J. Pan and C. Lin, *Corros. Sci.*, 51 (9) (2009) 2130-2138.
16. R. Liu, L. Jiang, J. Xu, C. Xiong and Z. Song, *Constr. Build. Mater.*, 56 (2014) 16-20.
17. L. Jiang, H. Liu, H. Chu, C. Zhu, C. Xiong, L. You, J. Xu, Y. Zhang and Y. Qin, *Constr. Build. Mater.*, 73 (2014) 699-704.
18. J. Wei, X.X. Fu, J.H. Dong and W. Ke, *J. Mater. Sci. Technol.*, 28 (10) (2012) 905-912.
19. S.P. Karthick, S. Muralidharan, V. Saraswathy and K. Thangavel, *Sens. Actuators B: Chem.*, 192 (2014) 303-309.
20. M. Jin, J. Xu, L. Jiang, G. Gao, H. Chu, C. Xiong, H. Gao and P. Jiang, *Electrochemistry*, 82 (12) (2014) 1040-1046.
21. M. Jin, L. Jiang, J. Xu, H. Chu, D. Tao, S. Bai and Y. Jia, *Electrochemistry*, 84 (6) (2016) 383-389.
22. S. Muralidharan, V. Saraswathy, K. Thangavel and N. Palaniswamy, *Sens. Actuators B: Chem.*, 130 (2) (2008) 864-870.
23. S. Muralidharan, V. Saraswathy, A. Madhavamayandi, K. Thangavel and N. Palaniswamy, *Electrochim. Acta*, 53 (24) (2008) 7248-7254.
24. S. Muralidharan, T.H. Ha, J.H. Bae, Y.C. Ha, H.G. Lee and D.K. Kim, *Measurement*, 40 (6) (2007) 600-606.
25. C.P. Atkins, M.A. Carter and J.D. Scantlebury, *Cem. Concr. Res.*, 31 (8) (2001) 1207-1211.
26. U. Angst, Ø. Vennesland and R. Myrdal, *Mater. Struct.*, 42 (3) (2009) 365-375.
27. Y. Choi, J. Kim and K. Lee, *Corros. Sci.*, 48 (7) (2006) 1733-1745.
28. H. Xu, Y. Liu, W. Chen, R. Du and C. Lin, *Electrochim. Acta*, 54 (16) (2009) 4067-4072.
29. C. Monticelli, M.E. Natali, A. Balbo, C. Chiavari, F. Zanotto, S. Manzi and M.C. Bignozzi, *Cem. Concr. Res.*, 80 (2016) 60-68.
30. M.A. Amin, S.S. Abd El-Rehim, E.E.F. El-Sherbini and R.S. Bayoumi, *Electrochim. Acta*, 52 (11) (2007) 3588-3600.
31. V.S. Ha-Won Song, *Int. J. Electrochem. Sci.*, 2 (2007) 1-28.
32. V. Shubina, L. Gaillet, T. Chaussadent, T. Meylheuc and J. Creus, *J. Clean. Prod.*, 112, Part 1

(2016) 666-671.
33. Ł. Sadowski, *Arch. Civ. Mech. Eng.*, 10 (2) (2010) 109-116.
34. M. Stern and A.L. Geary, *J. Electrochem. Soc.*, 104 (1) (1957) 56-63.
35. M.F. Montemor, A.M.P. Sim Es and M.G.S. Ferreira, *Cem. Concr. Compos.*, 25 (4–5) (2003) 491-502.
36. S. Ahmad, *Cem. Concr. Compos.*, 25 (4-5) (2003) 459-471.
37. D.A. Koleva, J.H.W. de Wit, K. van Breugel, Z.F. Lodhi and G. Ye, *J. Electrochem. Soc.*, 154 (5) (2007) C261-C271.
38. M. Jin, J. Xu, L. Jiang, Y. Xu and H. Chu, *Ionics*, 21 (2015) 2981-2992.
39. J.R. Scully, *Corrosion*, 56 (2) (2000) 199-218.
40. U. Angst, B. Elsener, C.K. Larsen and Ø. Vennesland, *J. Appl. Electrochem.*, 40 (3) (2010) 561-573.
41. U. Angst, B. Elsener, R. Myrdal and Ø. Vennesland, *Electrochim. Acta*, 55 (28) (2010) 8545-8555.
42. U. Angst and Ø. Vennesland, *Materials and Corrosion*, 60 (8) (2009) 638-643.
43. C. Bataillon and S. Brunet, *Electrochim. Acta*, 39 (3) (1994) 455-465.
44. K.Y. Ann and H. Song, *Corros. Sci.*, 49 (11) (2007) 4113-4133.
45. D.W. Law, J. Cairns, S.G. Millard and J.H. Bungey, *NDT&E Int.*, 37 (5) (2004) 381-388.
46. Z.P. Bazant, *Journal of the Structural Division*, 105 (6) (1979) 1137-1153.
47. S.J. Jaffer and C.M. Hansson, *Cem. Concr. Res.*, 39 (2) (2009) 116-125.